Geomechanics and Engineering, *Vol. 35, No. 3 (2023) 241-253*
https://doi.org/10.12989/gae.2023.35.3.241

Effect of initial static shear on liquefaction and pre-failure deformation of sand under bidirectional cyclic loading

Zhen-Dong Cui*, Tian-Yu Sui, Dong-Tai She and Li Yuan

State Key Laboratory for Geomechanics and Deep Underground Engineering, School of Mechanics and Civil Engineering, China University of Mining and Technology, Xuzhou, Jiangsu 221116, P. R. China

(*Received April 16, 2023, Revised September 25, 2023, Accepted October 6, 2023*)

Abstract. The effect of initial static shear τ_s on the dynamic characteristics of soil has been studied through extensive laboratory experiments over the past decades, but the influence of radial cyclic stress on its effect has rarely been considered. In this paper, a series of undrained triaxial tests were conducted to the saturated medium dense sand under axial and radial cyclic loadings with a phase difference of 180°. It is shown that the medium dense sand mainly performs two typical deformation response modes, including the accumulated plastic strain and cyclic mobility. The compressive static shear is conducive to the liquefaction resistance, while the extensional one is on the contrary. Such effects are magnified as p_0' increases, though the absolute value of *CRR* reduces. The radial cyclic load leads to a higher N_f compared with the loading in the single axial direction, and significantly affects the generation of the pore pressure and its relationship with the accumulation of the axial strain. The samples with the compressive static shear are more sensitive to the strain failure criteria. But for samples with extensional static shear, the limiting residual pore pressure ratio $u_{r,\,lim}$ precedes before the strain failure. For geotechnical applications, it is necessary to comprehensively consider both the pore pressure and strain failure criteria.

Keywords: cyclic resistance; cyclic triaxial tests; failure criterion; pore pressure; saturated sand; static shear; vertical earthquakes

1. Introduction

After 1964 Niigata earthquake and Alaska earthquakes, soil liquefaction has been widely concerned, becoming an important issue. Scholars have conducted a lot of research on the properties of liquefiable soils and improve them to protect the environment and the safety of structure construction (Hsiao and Phan 2014, Ghiasi and Mozafari 2018, Chou and Lin 2020, Sonmezer *et al.* 2020, Ghiasi and Hamedani 2022, Ghiasi and madah 2022). Moreover, soil elements at the bottom and edge of slopes, dams and structures are often acted by the additional static shear stress, which significantly impacts the dynamic characteristic of soils.

The effect of initial static shear τ_s on the dynamic characteristics of soils has been studied by many researchers. The initial shear was simulated with anisotropically consolidated samples by triaxial tests, following the early work of Lee and Seed (1967). After the anisotropic consolidation, the initial static deviatoric stress $q_s = \sigma_v - \sigma_h$, which induces the static shear stress $\tau_s = q_s / 2$ on the 45º plane of the triaxial samples. Based on this method, Lee and Seed (1967) found the initial static shear enhanced the cyclic strength of sand. However, the triaxial tests conducted by Vaid and Chern (1985) indicated that the liquefaction resistance could either increase or decrease with the effect of the τ_s and its trend resulted from the static shear level and the relative density of samples. The influence of the shear strain magnitude on the subsequent dynamic response of contractive sand was also studied. The liquefaction resistance increased with the small pre-shear strain increasing, but the pre-shearing beyond the phase transformation line had opposite effect (Vaid *et al*. 1989).

The effect of static shear was estimated based on the anticipated deformation characteristics of the sand, rather than the relative density (Vaid *et al*. 2004). Yang and Sze (2011) summed three deformation failure modes from a series of triaxial tests, including the flow-type failure, the cyclic mobility and the plastic strain accumulation. The threshold α was found to describe the effects of τ_s on the cyclic strength depending on the confining pressure and the relative density (Yang and Sze 2011). If α was lower than the threshold, the cyclic strength increased with the α increasing, while it decreased with α larger than the threshold (Yang and Sze 2011). The applicability of this theory for different types of sand such as Toyoura sand and Fujian sand was also tested (Yang and Sze 2011). Previous studies revealed that if there was initial static shear stress, the deformation was more likely to generate on the same side of τ_s (Hyodo *et al*. 1994). In addition, the excess pore water pressure (EPWP) also showed different behaviors. Under the cyclic loading, the EPWP generated and tended

*Corresponding author, Professor
E-mail: cuizhendong@cumt.edu.cn

ISSN: 2005-307X (Print), 2092-6219 (Online)

to approach the limited value which was always below the initial effective confining pressure, and the effective stress did not reach the zero effective stress state (Hyodo *et al*. 1994).

The experimental researches mentioned above mainly focused on the compressive static shear. However, the extensional static shear affected the soil elements away from the structures and it was more common for the offshore engineering. Andersen (2009) and Randolph (2012) investigated the influence of the extensional static shear preliminarily and the sand was more prone to large deformation. The extensional static shear weakened the cyclic resistance of samples (Pan and Yang 2018, 2017).

It is a well-established fact that the soil behavior is strongly dependent on the stress path. There were significant differences among the experimental results of the laboratory cyclic shear tests with different loading conditions (Vaid and Sivathayalan1996, Sivathayalan and Ha 2011). In the existing triaxial experimental research subject to τ_s, the cyclic load was applied in the single axial direction. Such simulation could excite corresponding cyclic shear on the 45º plane, but the cyclic stress was inevitably caused in the vertical direction of the plane which would significantly affect the soil response (Huang *et al*. 2011). Such problems can be solved by the bidirectional dynamic triaxial test. The amplitude and frequency of the radial cyclic load are the same as those of the axial one with a constant phase difference of 180°. The "bidirectional" here is different from other experimental methods. As for cyclic single shear tests, "bidirectional" was the combination of two shears perpendicular to each other in the same shear plane (Rasouli and Moradi 2021) and the cyclic shear was conducted for triaxial tests in one single direction.

In addition, the soil is usually affected by horizontal and vertical seismic motions during earthquakes. The recent research on the soil liquefaction behavior affected by τ_s mainly focused on the response under horizontal ground motions. However, the features of the vertical ground motions were pretty different from those of the horizontal ones (Yang *et al*. 2002). For example, their propagation were not weakened by the nonlinear behavior of soil, such as liquefaction (Bradley and Bradley 2011). The increment of the dynamic vertical stress was chiefly carried by the EPWP (Liu *et al*. 2018), which resulted in the high-frequency oscillation of the pore pressure (Tsaparli *et al*. 2016). The EPWP was an essential parameter for evaluating liquefaction and the impact of vertical motion on liquefaction should not be negligible (Yang 2004). Thus, it is necessary to study the response of the sand affected by the initial static shear under the bidirectional earthquake load.

In this study, a series of undrained bidirectional cyclic triaxial tests for the saturated medium dense sand were conducted to supplement the existing research. The vertical seismic effects were simulated by the radial cyclic load. Both the initial compressive and the extensional static shear were considered. The effects of τ_s on the deformation modes, the cyclic resistance and the pore water pressure development were studied under different initial mean effective stresses. The relationship between the *SSR* and the ultimate residual EPWP was presented and analyzed.

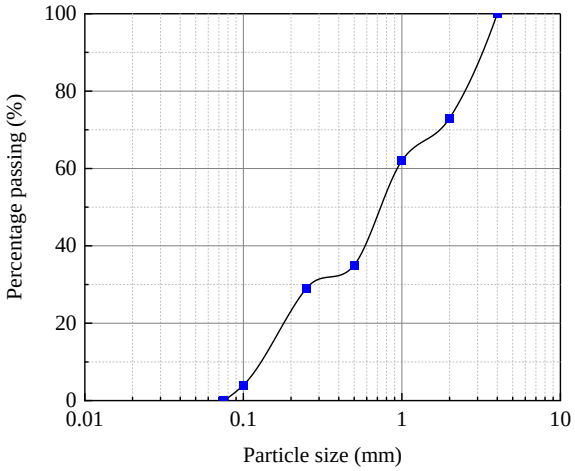

Fig. 1 Particle size distribution

2. Test procedure

This section describes the test apparatus, material and the sample prepare method used in this study.

2.1 Test apparatus

The bidirectional dynamic triaxial testing system developed by GDS was used in this study. This testing system comprises the pressure chamber, the servo host system, the hydraulic servo control loading system, analog and digital signal control systems, and the computer-controlled system. It is capable of isotropically and anisotropically consolidating, and loading in various modes. The most notable advantage of this device is that the dynamic loads in both axial and radial directions can be applied with the required stable phase difference.

2.2 Material and sample preparation

Fujian standard sand in China was used as the testing material. The basic physical properties are summarized in Table 1. Its maximum and minimum dry densities are 1.85 g/cm^3 and 1.61 g/cm^3, respectively. Fig. 1 illustrates the particle size distribution of Fujian standard sand. It is classified as SP (poorly graded sand) according to ASTM D2487. All the samples were prepared by the air pluviation method with the initial relative density D_r = 50%, 50 mm in diameter and 100 mm in height.

Each specimen was fully saturated in two stages. First, the specimens were flushed with the carbon dioxide and de-aired water. Then, back pressures with B-value checks were conducted until the B-values were greater than 0.95. After that, the specimens were isotropically consolidated. The target static shears τ_s were obtained in the subsequent anisotropic consolidation.

Table 1 Physical properties of Fujian standard sand

G_s	ρ_{max} (g/cm^3)	ρ_{min} (g/cm^3)	C_c	C_u
2.67	1.85	1.61	0.96	1.65

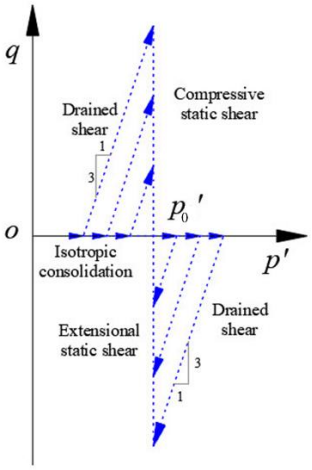

Fig. 2 Stress path prior to cyclic loading

In this study, both the extensional and the compressional initial static shear were discussed. For simplicity, the compressional and extensional static stresses are denoted as positive and negative, respectively, as shown in Fig. 2. The initial effective mean stress p_0' was set as 100 kPa and 300 kPa during the anisotropic consolidation, as shown in Eq. (1). The path of the drained consolidation stress was shown in Fig. 2 (Pan and Yang 2018).

$$p_0' = (\sigma_v' + 2\sigma_h')/3 \tag{1}$$

In the stress-control triaxial testing, different loading requirements are performed by coupling the initial static deviator stress q_s and the bidirectional cyclic load. In this study, the bidirectional sinusoidal cyclic load of 1Hz with the same amplitude and phase difference 180° is selected. The shear stress ratio (*SSR*) and cyclic stress ratio (*CSR*) are used to control the loading value, defined as Eqs. (2) and (3).

$$SSR = \tau_s / p_0' = q_s / (2p_0') = (\sigma_v' - \sigma_h')/(2p_0') \tag{2}$$

$$CSR = q_{cyc} / p_0' \tag{3}$$

The total axial applied load is defined as Eq. (4).

$$q(t) = q_s + q_{cyc}\sin(2\pi ft) \tag{4}$$

where q_s is the static deviatoric stress; q_{cyc} is the amplitude of cyclic deviatoric stress; f is the loading frequency and t is time. If $q_{cyc} > \tau_s$ (CSR>SSR), it is considered as stress reversal, on the contrary, no reversal. All cyclic tests were carried out in undrained conditions. The test program is shown in Table 2. It is worth noting that the application of

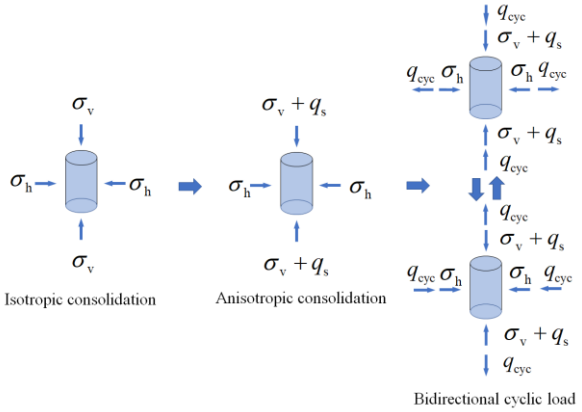

Fig. 3 Diagram of the loading process

Table 1 Undrained cyclic triaxial test program

Series	σ_v' (kPa)	σ_h' (kPa)	q_s (kPa)	*SSR*	*CSR*	q_s/q_{cyc}
I	100	100	0	0	0.125	0
	100	100	0	0	0.25	0
II	114	94	20	0.1	0.125	0.8
	114	94	20	0.1	0.15	0.67
	114	94	20	0.1	0.2	0.5
	114	94	20	0.1	0.25	0.4
III	134	84	50	0.25	0.175	1.43
	134	84	50	0.25	0.2	1.25
	134	84	50	0.25	0.225	1.11
	134	84	50	0.25	0.3	0.83
IV	154	74	80	0.4	0.25	1.6
	154	74	80	0.4	0.275	1.45
	154	74	80	0.4	0.3	1.33
	154	74	80	0.4	0.35	1.14
V	94	104	-10	-0.05	0.1	-0.5
	94	104	-10	-0.05	0.15	-0.33
	94	104	-10	-0.05	0.2	-0.25
VI	87	107	-20	-0.1	0.075	-1.33
	87	107	-20	-0.1	0.1	-1
	87	107	-20	-0.1	0.15	-0.66
VII	73	113	-40	-0.2	0.1	-4
	73	113	-40	-0.2	0.125	-3
	73	113	-40	-0.2	0.15	-2.4
VIII	60	120	-60	-0.3	0.1	-4
	60	120	-60	-0.3	0.15	-3
	60	120	-60	-0.3	0.2	-2.4
b-I	300	300	0	0	0.075	0
	300	300	0	0	0.1	0
	300	300	0	0	0.125	0
b-II	340	280	60	0.1	0.1	1
	340	280	60	0.1	0.125	0.8
	340	280	60	0.1	175	0.57
b-III	400	250	150	0.25	0.175	2
	400	250	150	0.25	0.2	1.67
	400	250	150	0.25	0.225	1.5
b-IV	460	220	240	0.4	0.175	2.29
	460	220	240	0.4	0.225	1.78
	460	220	240	0.4	0.25	1.6
b-V	280	310	-30	-0.05	0.1	-0.5
	280	310	-30	-0.05	0.125	-0.4
	280	310	-30	-0.05	0.15	-0.33
b-VI	260	320	-60	-0.1	0.075	-1.33
	260	320	-60	-0.1	0.1	-1
	260	320	-60	-0.1	0.125	-0.8

radial load is achieved by the vibration of the confining pressure, which is a cyclic spherical stress $\sigma_3^{cyc} = q_{cyc}$. When the phase difference between the axial and radial loads is

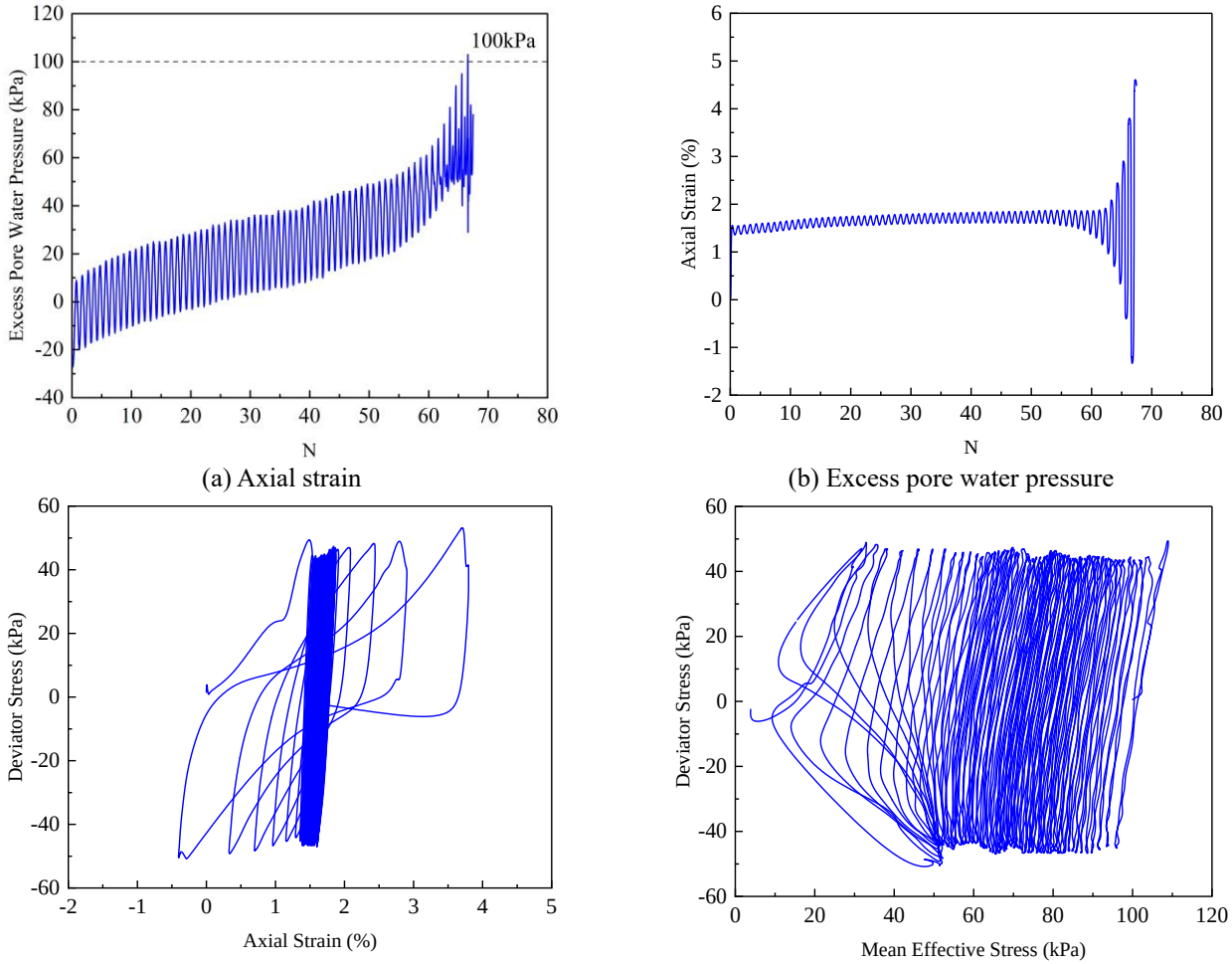

(a) Axial strain (b) Excess pore water pressure

(c) Stress strain curve (d) Effective stress path

Fig. 4 Cyclic response of medium dense sand for p_0' being 100 kPa, *SSR* being 0 and *CSR* being

fixed at 180°, the cyclic spherical stress will partially offset and weaken the axial load applied to the test. Attention should be paid during the test control to avoid the situation where the actual force of the soil sample cannot reach the target stress. Fig. 3 illustrates the diagram of the consolidation and loading process.

3. Test results

The test results of the cyclic triaxial tests on saturated sand samples are presented and analyzed in this section. The discussion will be carried out from the following aspects: deformation mode, cyclic resistance, pore water pressure development and pre-failure deformation.

3.1 Cyclic response and deformation modes

Figs. 4-7 illustrate the typical cyclic response of the saturated medium dense samples with or without the compressive static shear, including the EPWP, the axial strain, the stress-strain curve and the effective stress path.

From the perspective of the strain development of the sample, the deformation mode of the sample can be divided into three types, including the cyclic mobility, the accumulated plastic strain and the flow-type failure.

Fig. 4 shows the typical cyclic response of a medium dense sample with p_0' being 100 kPa, SSR being 0 and CSR being 0.25. In the first 59 cycles with the EPWP gradually increasing, the effective stress decreases (Figs. 4(a), 4(d)), and the axial strain is negligible except for 1.3% strain in the first cycle (Fig. 4(b)). After *N*=60, the EPWP increases rapidly trending to approach the initial effective confining pressure. Simultaneously, the double amplitude axial strain rapidly develops and exceeds 5%, resulting in the "S-shaped" stress-strain curve. When *N*=66, the average effective stress tends to be the near-zero effective stress state with the typical "butterfly" stress path. This kind of response mode is cyclic mobility. Compared with Yang and Pan (2018) under a similar stress situation for p_0' being 100 kPa, SSR being 0 and CSR being 0.2 whose axial strain exceeds 6% at the 26th cycle, though the sample is looser and the cyclic load is higher, it needs more cycles to reach failure under the bidirectional cyclic loading.

Fig. 5 presents the cyclic response of sample for p_0' being 100 kPa, SSR being 0.25 and CSR being 0.175. It is significantly different from the cyclic mobility one shown in Fig. 4. The residual pore pressure is built up stably

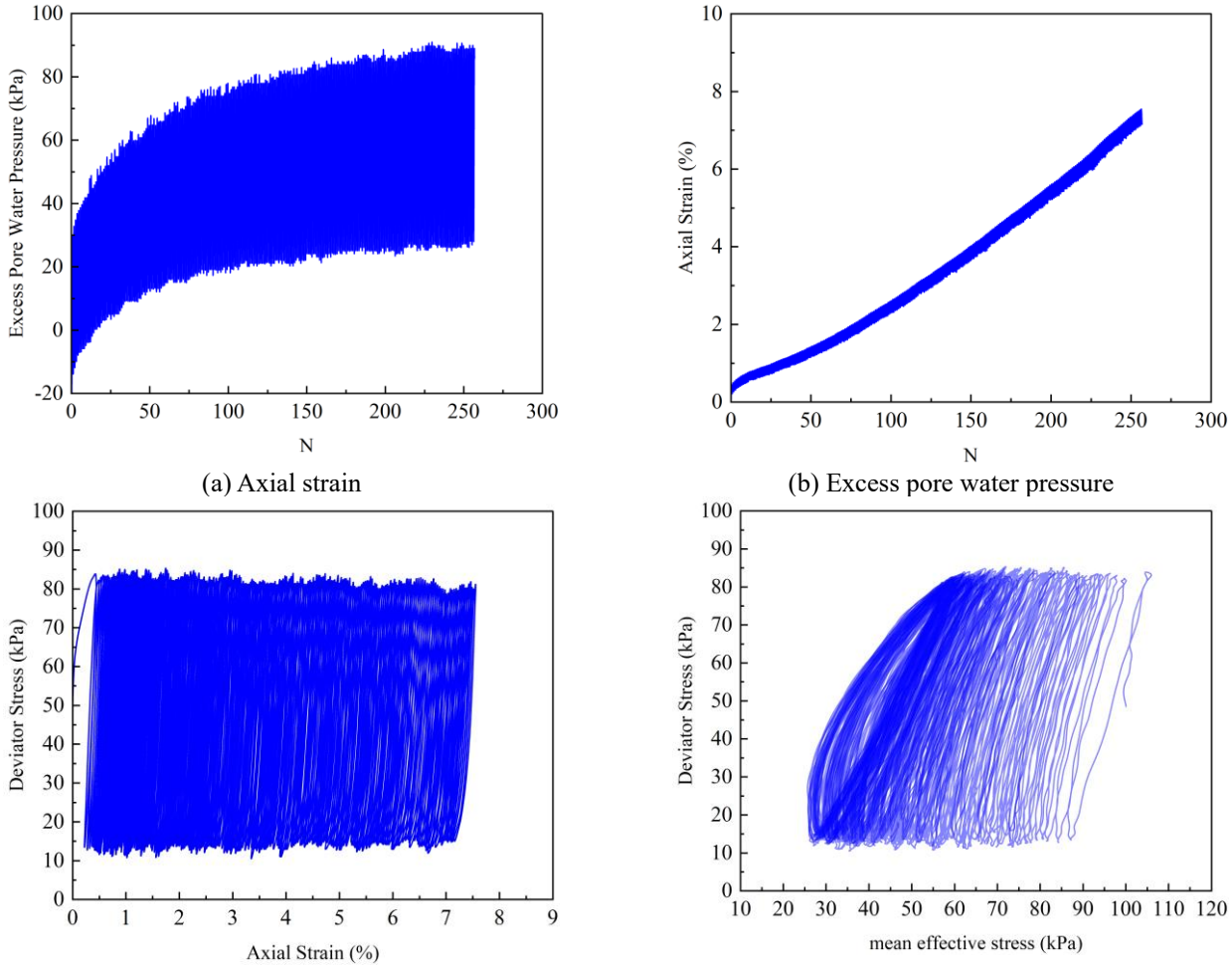

(a) Axial strain (b) Excess pore water pressure

(c) Stress strain curve (d) Effective stress path

Fig. 5 Cyclic response of medium dense sand for p_0' being 100 kPa, *SSR* being 0.25 and *CSR* being 0.175

during the dynamic loading process. It tends to the limiting value below the initial effective confining pressure at about 60 kPa with a rate slowing down gradually and the amplitude of the transient pore water pressure (PWP) increases slowly (Fig. 4(a)). Accordingly, the effective stress reduces with the PWP increasing. It cannot reach the zero-stress state (Fig. 5(d)). The stress path takes the skewed lens shape before failure (Liu *et al*. 2021). Fig. 5(b) shows that the strain accumulation arises on the compressive side (the same as the static shear) and eventually exceeds 5% at the 68th cycle. This kind of deformation mode is called accumulated plastic strain. As for the stress-strain curve shown in Fig. 5(c), although the shape of the hysteresis curve is almost unchanged, its center moves with the strain.

Fig. 6 and 7 illustrate the similar behavior for samples affected by the extensional static shear. The former (p_0' = 300 kPa; *SSR* = -0.05; *CSR*=0.1) belongs to the cyclic mobility, while the latter (p_0' = 100 kPa; *SSR* = -0.2; *CSR*=0.125) belongs to the accumulated plastic strain. But in contrast, the samples affected by extensional static shear stress experience a more rapid process of deformation development, and the strain tends to develop on the extensional side. As shown in Figs. 5 and 7, their stress levels are equivalent except for the different directions of the τ_s. The strain induced by the extensional static shear reaches 5% in the 23rd cycle, while the sample influenced by the initial compressive shear undergoes 190 cycles before reaching the same strain level.

In addition, with the influence of extensional static shear, the flow-type failure of the sample is caused by some load combinations, as shown in Fig. 8. The EPWP of the medium dense saturated sand sample increases suddenly and approaches the p_0' in the first 3 cycles (Figs. 8(a), 8(d)). The effective stress is almost depleted, reaching the near-zero stress state. The axial strain shown in Fig. 8(b) develops sharply and instantly exceeds 20% on the extensional side in the 4th cycle. It is also perceptible that the kind of sand, loose or dense, should be discussed in the context of the p_0'. The flow-type failure is more likely to appear under high-stress conditions even if the sand has the same relative density (Yang *et al*. 2022).

Judging from the tests conducted in this paper, the flow-type failure rarely appears, so the cyclic mobility and the accumulated plastic strain are discussed as follows.

The above analysis shows that the deformation mode of sand under various conditions depends on the value and

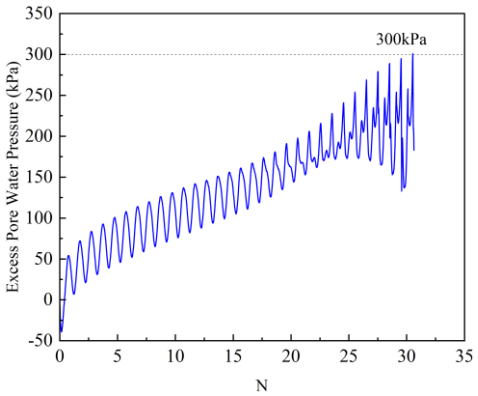

(a) Axial strain

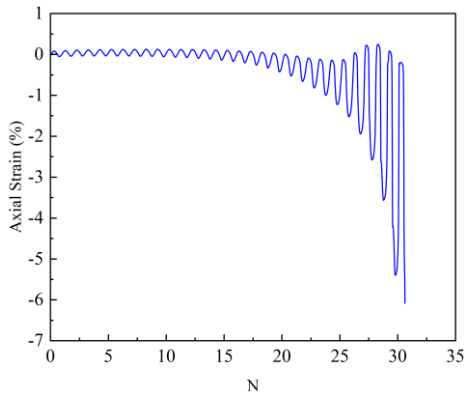

(b) Excess pore water pressure

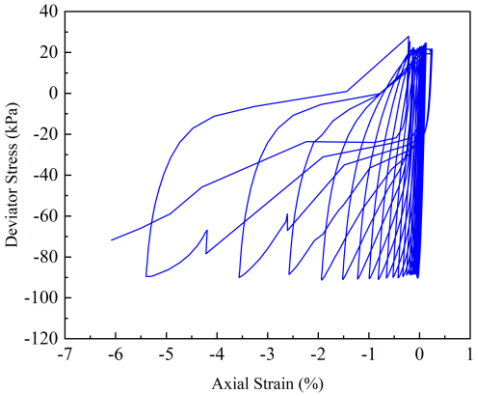

(c) Stress strain curve

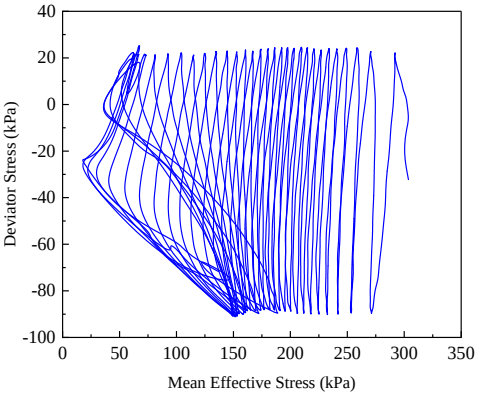

(d) Effective stress path

Fig. 6 Cyclic response of medium dense sand for p_0' being 300 kPa, *SSR* being -0.05 and *CSR* being 0.1

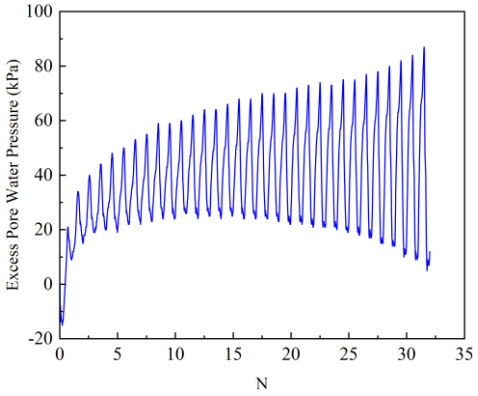

(a) Axial strain

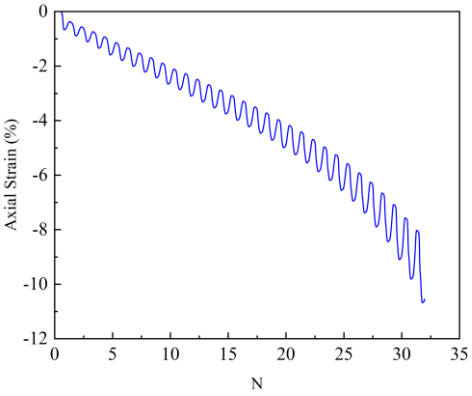

(b) Excess pore water pressure

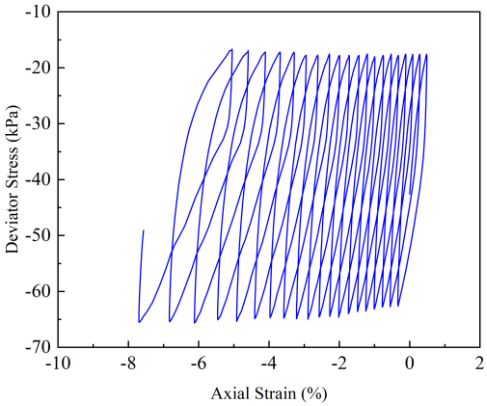

(c) Stress strain curve

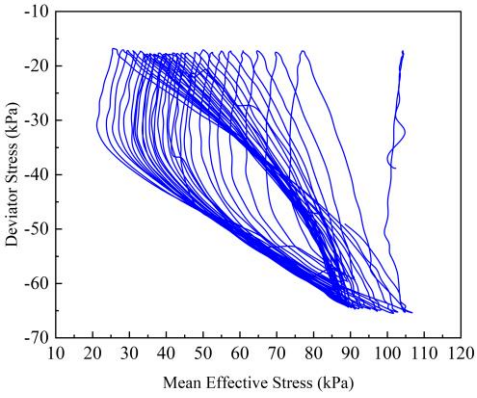

(d) Effective stress path

Fig. 7 Cyclic response of medium dense sand for p_0' being 100 kPa, *SSR* being -0.2 and *CSR* being 0.125

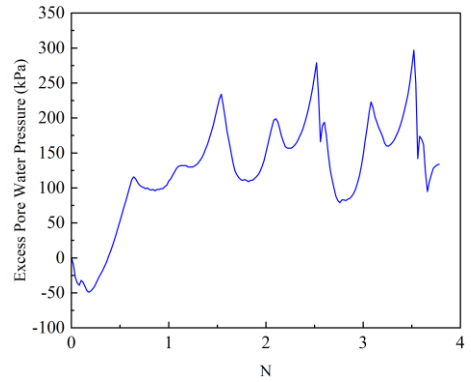

(a) Axial strain

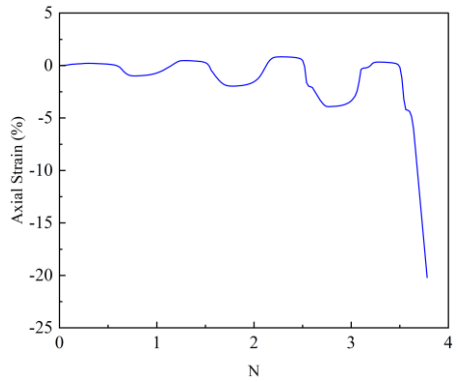

(b) Excess pore water pressure

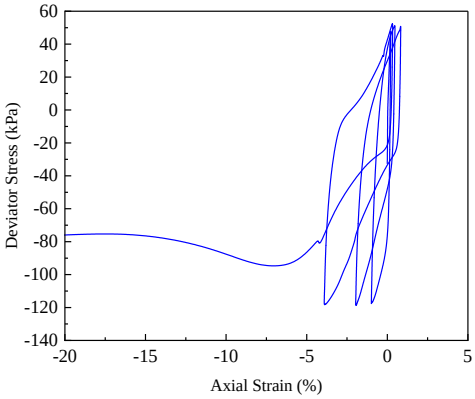

(c) Stress strain curve

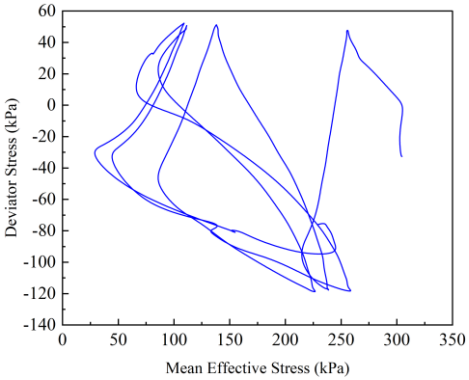

(d) Effective stress path

Fig. 8 Cyclic response of medium dense sand for p_0' being 300 kPa, *SSR* being -0.05 and *CSR* being 0.15

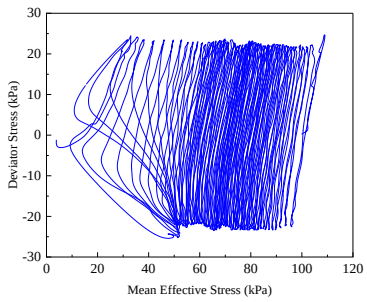

(a) $SSR = 0$; $CSR = 0.125$

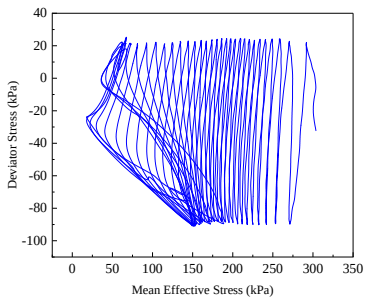

(b) $SSR = -0.05$; $CSR = 0.1$

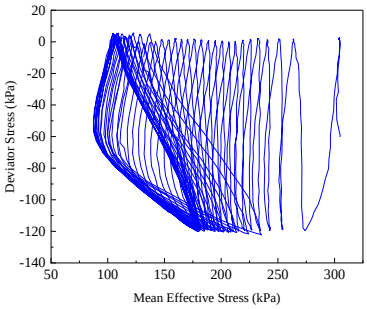

(c) $SSR = -0.1$; $CSR = 0.1$

Fig. 9 Effects of initial static shear magnitudes on stress path

sign of the τ_s. As shown in Fig. 9, with the same *CSR*, as the absolute value of SSR increases, the effective stress path at the compressive side decreases, gradually evolving from a butterfly with symmetrical wings on both compressive and extensional sides to which has only one wing on the extensional side.

Fig. 10 illustrates the variations of *SSR* with *CSR*, which is divided into three zones by two reference lines, showing the cyclic behavior of the medium dense sand. The deformation mode of the samples is closely related to where the load combination is in these three zones. If $q_s / q_{cyc} > 1.2$ or $q_s / q_{cyc} < -0.8$, the sample destruction is caused by the accumulated plastic strain. If $-0.8 < q_s / q_{cyc} < 1.2$, the samples exhibit the cyclic mobility. The deformation mode of samples shows the accumulated plastic strain with the

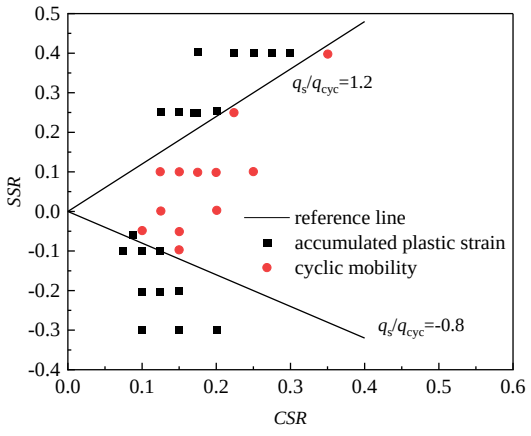

Fig. 10 Cyclic response behavior of medium dense sand under different stress conditions

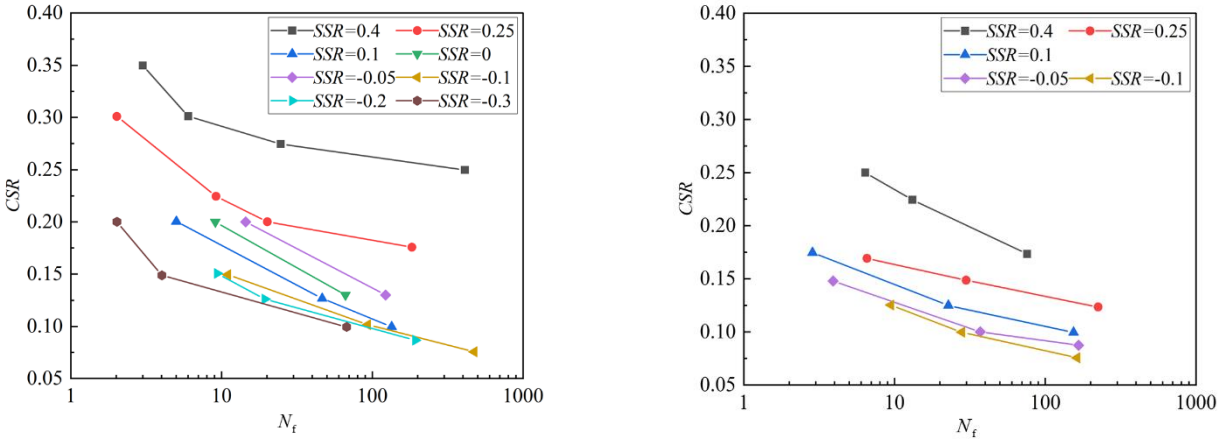

(a) p_0' = 100 kpa (b) p_0' = 300 kpa

Fig. 11 Variations of N_f with *CSR*s and *SSR*s under different initial mean effective stresses

larger static deviator stress. However, the cyclic response mode is more likely to manifest as the cyclic mobility with the smaller static deviator stress.

3.2 Cyclic Resistance with strain criterion

In dynamic triaxial tests, 5% of the single axial strain was often used as the destruction standard of samples (Yang and Sze 2011, Masayuki *et al*. 2002, Vaid *et al*. 2001). For the cyclic mobility of samples, achieving 5% of the single axial strain is difficult. Considering the development of PWP, 5% of the double axial strain was defined as the destruction standard (Ishihara 1996). For the accumulated plastic strain, 5% of the single axial strain was still used. The cycles N_f for the axial strain reaching the failure standard were defined as the number of cycles for failure (Pan and Yang 2018).

Fig. 11 illustrates the variations of *CSR* with N_f under different initial effective mean stresses. For the same *SSR*, N_f increases with the *CSR* decreasing. The soil is subject to a larger dynamic load, which is more unstable and easier to reach the destruction criteria. The dynamic strength is also related to the relative value and direction of the static deviator stress. For the same *CSR*, N_f increases with the *SSR* decreasing. It can also be observed that the N_f - *CSR* curves affected by the extensional static shear are closer, which shows that the dynamic strength of the medium dense sand is less sensitive to the extensional static shear.

To quantify the influence of the τ_s on the dynamic strength of the medium dense sand, the cyclic resistance ratio CRR_n was defined as the cyclic stress ratio *CSR* required to reach the destruction criteria at the 10th loading cycle (N_f = 10) (Ishihara 1993, Konstadinou and Georgiannou 2013). As shown in Fig. 12, for any given *SSR*, the *CRR* of the sand with p_0' - 100 kPa is generally higher than that with p_0' = 300 kPa. For the similar trend of variations of CRR_n with *SSR* under different mean effective stresses, K_α was introduced to reflect the relative change of the liquefaction resistance of samples (Seed 2011). K_α is

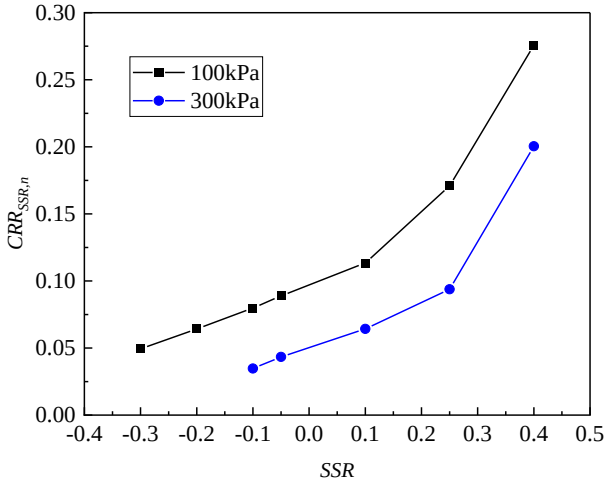

Fig. 12 Variations of the $CRR_{SSR,n}$ with *SSR* under different effective stresses

the ratio of $CRR_{SSR,n}$ at any *SSR* to $CRR_{0,n}$ with *SSR* being 0, as shown in Eq. (5). As shown in Fig. 13, with *SSR* being 0, K_α =1. The initial extensional static shear results in the weakening of the dynamic strength with K_α less than 1.

On the contrary, the compression static shear enhances the sand with K_α larger than 1. This effect is more obvious when the p_0' increases. The trend is related to the initial relative density of samples (Yang and Sze 2011).

$$K_\alpha = \frac{CRR_{SSR,n}}{CRR_{0,n}} \tag{5}$$

3.3 Pore water pressure development

The EPWP generated in soil samples during the cyclic loading can be separated into two components, including the transient EPWP and the residual EPWP (Polito *et al*. 2008). The former refers to the real-time EPWP, having little effect on the effective stress of the soil. However, the latter means the part that cannot dissipate in time at the end

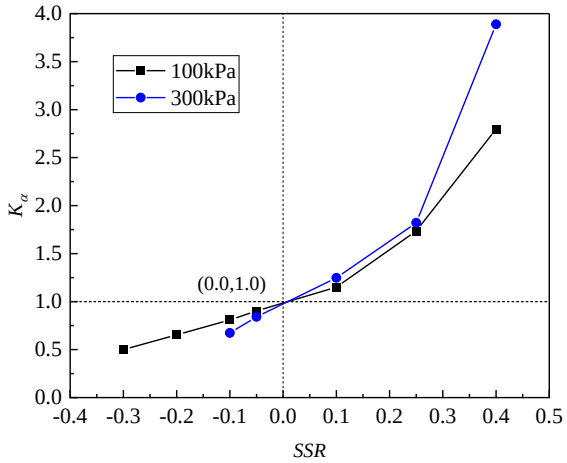

Fig. 13 Variations of K_α with *SSR* under different confining pressure

of every loading cycle, accumulating and altering the effective stress during the cyclic loading (Kammerer *et al.* 2005), which directly affects the stiffness and strength of the soil.

As shown in Figs. 4 and 8, the transient EPWP is less than 0 in the first half of the loading cycle, which is caused by the loading method. Due to the phase difference of 180° in the axial and radial cyclic loading, the axial load on the soil sample is compressive in the first half of each cycle, and that of the radial load is extensional. In addition, the radial load is applied through the periodic changes of the confining pressure, which directly reflects the transient pore pressure. If the increase of the pore pressure caused by the dynamic load is less than that caused by the confining pressure, the transient EPWP appears as a negative value. For saturated sand samples, the change of the transient pore pressure is equal to that of the confining pressure. The residual excess pore water pressure ratio u_r is defined as the ratio of the residual EPWP to the p_0'. There exist limited values of EPWPs under the initial static shear, so u_r also has limited values $u_{r,\,lim}$ Fig. 14 illustrates the variations of the limiting pore water pressure ratio $u_{r,\,lim}$ and *SSR* under different cyclic stress ratios *CSR*. From Fig. 14(a), the effective accumulation of EPWP does not arise with the *CSR* being too small relative to the *SSR*, such as points (*SSR*=0.1, *CSR*=0.1) and (*SSR*=0.4, *CSR*=0.25), and the $u_{r,\,lim}$ almost depends on the SSR, hardly affected by *CSR* with *SSR* between -0.3 and 0.4. The $u_{r,\,lim}$ increases with *SSR* from -0.3 to 0. However, when *SSR*>0, the $u_{r,\,lim}$ decreases with the *SSR*, which agrees well with Pan and Yang (2018). This phenomenon is related to the distance between the initial stress state and the critical state line CSL. As the horizontal distance between the initial stress state and the CSL becomes shorter with the increase of the absolute value of the *SSR*, the $u_{r,\,lim}$ has a tendency to decrease (Pan and Yang 2018, Liu *et al.* 2021), which is related to the consolidation process. As mentioned earlier, the samples are firstly isotropically consolidated under target confining stresses σ_h' and then applied axial compressive or extensional static loads to simulate initial

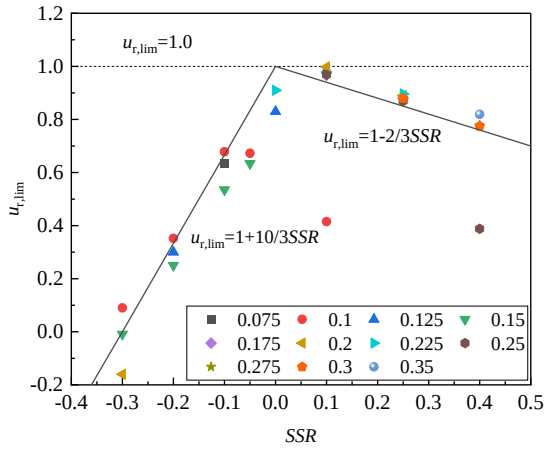

(a) p_0' = 100 kpa

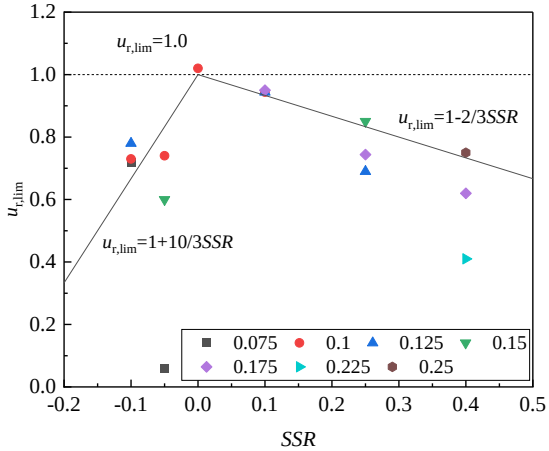

(b) p_0' = 300 kpa

Fig. 14 Variations of the $u_{r,\,lim}$ and *SSR* under different *CSR*s

static shears. For a given *SSR*, the stress applied axially and radially during consolidation is calculated with Eqs. (1) and (2) where σ_h' = (1-2/3*SSR*) p_0' and σ_v' = (1+4 /3*SSR*) p_0'. It is also perceptible that the ultimate residual EPWPs are always close to the confining pressures during the isotropic consolidation with *SSR*>0, therefore $u_{r,\,lim}$=1-2/3*SSR* as shown in Fig. 14. Similarly, when *SSR*<0, $u_{r,\,lim}$=1+10/3*SSR*.

3.4 Pre-failure deformation

For the liquefiable ground, the pre-failure deformation of soil is important for the serviceability of structures under the cyclic loading. The direction of strain accumulation of sand under the drained cyclic loading had been studied in previous research (Chang and Whitman 1988, Wichtmann and Niemunis 2006, Liu *et al.* 2021). The initial τ_s also affects the accumulation process of the residual axial strain ε_{ar} of samples with the residual excess pore pressure u_r.

Fig. 15 shows the accumulation process and development of ε_{ar} with the residual pore pressure of the sample under p_0' = 100 kpa. As shown in Fig. 15(a), ε_{ar} tends to develop on the compressive side with *SSR*>0.

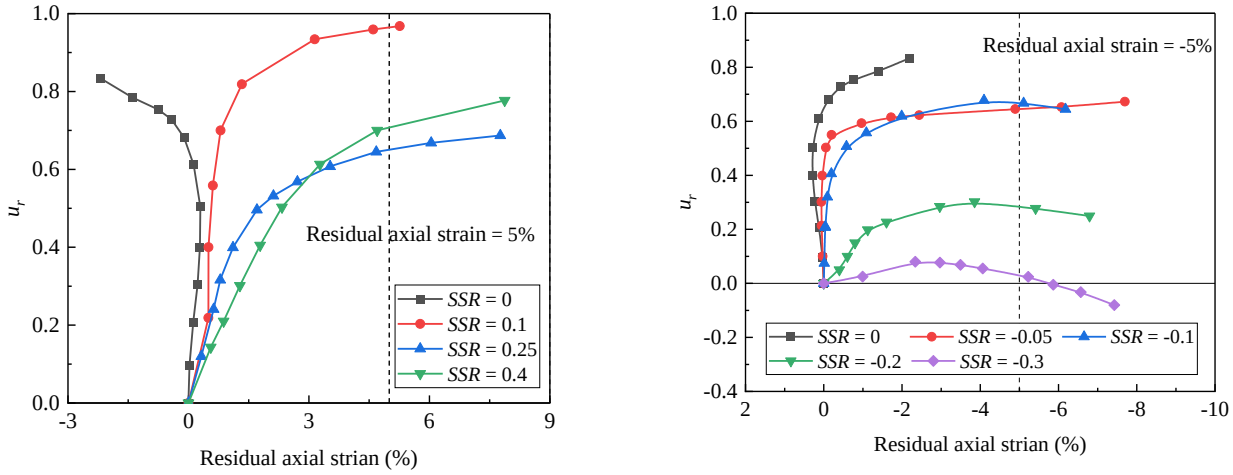

(a) $SSR \geq 0$ (b) $SSR \leq 0$

Fig. 15 Variation of the residual axial strain with the EPWP ratio for p_0' being 100 kPa

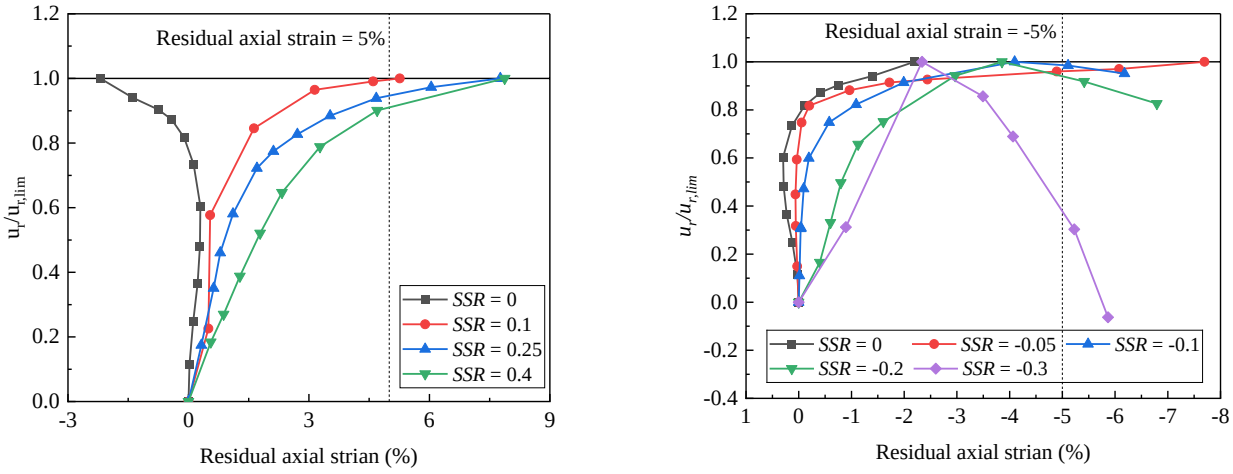

(a) $SSR \geq 0$ (b) $SSR \leq 0$

Fig. 16 Variation of the residual axial strain with the normalized EPWP ratio for p_0' being 100 kPa

Before u_r grows to 0.5, the ε_{ar} of the sample with higher *SSR* develops faster and the u_r grows rapidly with ε_{ar}.

When $u_r = 0.5$, the ε_{ar} of samples with *SSR* being 0, 0.1, 0.25 and 0.4 is 0.30%, 0.54%, 1.76% and 2.24%, respectively. The rate of the increase of u_r slows as ε_{ar} grows. After ε_{ar} = 3%, the u_r of the sample with *SSR*=0.4 exceeds that of the sample with *SSR*=0.25. Compared with the research results presented by Liu *et al*. (2021), the samples subjected to the radial cyclic loads are more prone to deformation. In their study, the ε_{ar} shows an inflect point after $u_r = 0.6$ and the rises rapidly without the static shear stress, while in this study, this phenomenon occurs when $u_r = 0.5$. Other specimens affected by the compressive static shear have similar characteristics under the bidirectional cyclic load.

To further study the relationship between the accumulation process of pore pressure and residual strain, the residual pore pressure is normalized, as shown in Fig. 16. Obviously, in the accumulation process of u_r from 0 to $u_{r,\,lim}$ ($u_r/u_{r,\,lim}$ from 0 to 1), as the *SSR* grows, the corresponding u_r becomes smaller for reaching the same residual strain. That is to say, under the bidirectional cyclic load, compared with the pore pressure failure criterion, samples are more likely to meet the strain failure criterion. Moreover, the growth rate of residual axial strain of samples accelerates with the development of u_r.

For *SSR* less than 0, the samples experience large strains when the increment of pore pressure is small. This phenomenon is more obvious with the smaller *SSR*. For *SSR* being -0.05 and -0.1, with -2% axial residual strain samples, the u_r reaches more than 0.6, while for *SSR* being -0.2, the corresponding u_r is only 0.21, and for *SSR* being -0.3, it is only 0.06. In addition, with *SSR* decreasing, the u_r has an extreme value at the middle stage of the ε_{ar} development. It decreases or even has a negative value at the later stage of the extensional strain generation. As shown in Fig. 16(b), the ε_{ar} at which the u_r reaches its peak $u_{r,\,lim}$ increases and then decreases with *SSR*. The absolute value of ε_{ar} is less than 5% for the samples with SSR being -0.3, -0.2 and -0.1 arriving $u_{r,\,lim}$. In other word, they trigger the pore pressure

failure criterion first.

Under the influence of bidirectional cyclic loads, the samples with compressive static shear will trigger strain failure criteria first, while for those with extensional static shear the sample failure gradually changes first-trigger strain failure criteria to first-trigger pore pressure failure criteria. It is still necessary to comprehensively consider the pore pressure and strain failure criteria of samples.

5. Conclusions

A series of undrained triaxial tests for the saturated medium dense sand were conducted to study the influence of initial static shears on the sand behavior under bidirectional cyclic loads considering the effect of vertical ground motions. The axial strain development, pore pressure generation, strength characteristics and pre-failure deformation were analyzed. The results are as follows.

- Under bidirectional cyclic loads, the medium dense sand mainly performs two typical deformation response modes: including the accumulated plastic strain and the cyclic mobility, which are related to the relative magnitude of the q_s and the cyclic load amplitude q_{cyc}. The accumulated plastic strain is more likely to appear with larger $\left|q_s/q_{cyc}\right|$, and the possibility of cyclic mobility is greater with smaller $\left|q_s/q_{cyc}\right|$.
- The number of cycles to failure N_f is related to the *CSR*, *SSR* and p_0'. For a given *CSR*, the required N_f increases with the *SSR* increasing. The compressive static shear benefits the cyclic resistance of medium dense sand, while the extensional one is on the contrary. Such effects are magnified as p_0' increases, though the absolute value of *CRR* reduces. In addition, the bidirectional cyclic load leads to a higher N_f compared with the loading in the single axial direction.
- Depending on the *SSR*, the residual pore pressure ratio reaches the limiting value of less than 1.0 under the bidirectional cyclic loading. For *SSR* less than 0, the $u_{r,lim}$ increases with the *SSR* increasing but decreases for the *SSR* larger than 0. The trend of $u_{r,lim}$ concerning for to *SSR* is not associated with the cyclic stress amplitude.
- For *SSR* larger than 0, the stains exceeding the failure criteria occurs before the sample reaches. At the same time, for *SSR* less than 0, the residual pore pressure has an extreme value at the middle stage of strain development. It will begin to decrease or even has the negative value at the later generation stage of extensional strain. For geotechnical applications with initial static shear stress in soil, it is necessary to comprehensively consider both the pore pressure failure criteria and the strain failure criteria.

Acknowledgments

The work presented in this paper was funded by National Natural Science Foundation of China (Grant No. 52378381).

References

Andersen, K.H. (2009), "Bearing capacity under cyclic loading — offshore, along the coast, and on land", *Can. Geotech. J.*, **46**(5), 513-535. https://doi.org/10.1139/T09-003.

Bradley, B.A. and Cubrinovski, M. (2011), "Near-source Strong Ground Motions Observed in the 22 February 2011 Christchurch Earthquake", *Seismol. Res. Lett.*, **82**(6), 853-865. https://doi.org/10.1785/gssrl.82.6.853.

Chang, C.S. and Whitman, R.V. (1988), "Drained permanent deformation of sand due to cyclic loading", *J. Geotech. Eng.*, **114**(10), 1164-1180. https://doi.org/10.1061/(ASCE)0733-9410(1988)114:10(1164).

Chou, J.C. and Lin, D.G. (2020), "Incorporating ground motion effects into Sasaki and Tamura prediction equations of liquefaction-induced uplift of underground structures", *Geomech. Eng.*, **22**(1), 25-33. https://doi.org/10.12989/gae.2020.22.1.025.

Ghiasi, V. and Madah, S. (2022), "Investigation of increasing shear strength of dispersive clays using additives", *Road*, https://doi.org/10.22034/road.2022.324512.2023.

Ghiasi, V. and Mozafari, V. (2018), "Seismic response of buried pipes to microtunnelling method under earthquake loads", *Soil Dyn. Earthq. Eng.*, **113**, 193-201. https://doi.org/10.1016/j.soildyn.2018.05.020.

Ghiasi, V. and Tavagho Hamedani, H. (2022), "A review of soil improvement with waste and recycled materials and its impact on soil parameters", *Road*, https://doi.org/10.22034/road.2022.324228.2019.

Hsiao, D.H. and Phan, V.T.A. (2014), "Effects of silt contents on the static and dynamic properties of sand-silt mixtures", *Geomech. Eng.*, **7**(3), 297-316. https://doi.org/10.12989/gae.2014.7.3.297.

Huang, B., Hu, J.Q., Shi, M.X. and Chen, Y.M. (2011), "Comparison of dynamic properties of saturated sand under unidirectional and two-directional cyclic triaxial tests conditions", *China Earthq. Eng. J.*, **33**(1), 137-142.

Hyodo, M., Tanimizu, H., Yasufuku, N. and Murata, H. (1994), "Undrained cyclic and monotonic triaxial behaviour of saturated loose sand", *Soils Found.*, **34**(1), 19-32. https://doi.org/10.3208/sandf1972.34.19.

Ishihara, K. (1993), "Liquefaction and flow failure during earthquakes", *Geotechnique*, **43**(3), 351-415. https://doi.org/10.1680/geot.1993.43.3.351.

Ishihara, K. (1996), Soil Behaviour In Earthquake Geotechnics, Clarendon Press,Oxford, UK.

Kammerer, A.M., Pestana, J.M. and Seed, R.B. (2005), "Behavior of monterey 0/30 sand under multidirectional loading conditions", First Japan-U.S. Workshop on Testing, Modeling, and Simulation, Boston, June

Konstadinou, M. and Georgiannou, V.N. (2013), "Cyclic behaviour of loose anisotropically consolidated Ottawa sand under undrained torsional loading", *Geotechnique*, **63**(13), 1144-1158. https://doi.org/10.1680/geot.12.P.145.

Lee, K.L. and Seed, H.B. (1967), "Dynamic strength of anisotropically consolidated sand", *J. Soil Mech. Found. Division*, **93**(5), 169-190. https://doi.org/10.1061/JSFEAQ.0001019.

Liu, X.., Wang, R. and Zhang, J.M. (2018), "Centrifuge shaking table tests on 4 × 4 pile groups in liquefiable ground", *Acta Geotech.*, **13**(6), 1405-1418. https://doi.org/10.1007/s11440-018-0699-5.

Liu, Z., Xue, J. and Ye, J. (2021), "The effects of unloading on drained cyclic behaviour of Sydney sand", *Acta Geotech.*, **16**(9), 2791-2804. https://doi.org/10.1007/s11440-021-01209-6.

Liu, Z.Y., Qian, J.G., Yaghoubi, M. and Xue, J.F. (2021), "The effects of initial static deviatoric stress on liquefaction and pre-

failure deformation characteristics of saturated sand under cyclic loading", *Soil Dyn. Earthq. Eng*., **149**(2), 106870. https://doi.org/10.1016/j.soildyn.2021.106870.

Masayuki, H., Adrian, F.L.H., Noritaka, A. and Yukio, N. (2002), "Undrained monotonic and cyclic shear behaviour of sand under low and high confining stresses", *Soils Found*., **42**(3), 63-76. https://doi.org/10.3208/sandf.42.3_63.

Pan, K. and Yang, Z.X. (2018), "Effects of initial static shear on cyclic resistance and pore pressure generation of saturated sand", *Acta Geotech.*, **13**(2), 473-487. https://doi.org/10.1007/s11440-017-0614-5.

Polito, C.P., Green, R.A. and Lee, J. (2008), "Pore pressure generation models for sands and silty soils subjected to cyclic loading", *J. Geotech. Geoenviron. Eng*., **134**(10), 1490-1500. https://doi.org/10.1061/(asce)1090-0241(2008)134:10(1490).

Randolph, M.F. (2012), Offshore Design Approaches and Model Tests for Sub-Failure Cyclic Loading of Foundations, Springer, Vienna, Austria.

Rasouli, M.R., Moradi, M. and Ghalandarzadeh, A. (2021), "Effects of initial static shear stress orientation on cyclic behavior of calcareous sand", *Mar. Georesour. Geotec*., **39**(5), 554-568. https://doi.org/10.1080/1064119x.2020.1726535.

Seed, H. (2011), "Earthquake-resistant design of earth dams", Can. *Geotech. J*., **4**(1), 1-27. https://doi.org/10.1139/t67-001.

Sivathayalan, S. and Ha, D. (2004), "Effect of initial stress state on the cyclic simple shear behaviour of sands", *Proceedings of the International Conference on Cyclic Behaviour of Soils and Liquefaction Phenomena*, Bochum, Germany, Mar 31-Apr 02

Sivathayalan, S. and Ha, D. (2011), "Effect of static shear stress on the cyclic resistance of sands in simple shear loading", *Can. Geotech. J.*, **48**(10), 1471-1484. https://doi.org/10.1139/t11-056.

Sonmezer, Y.B., Akyuz, A. and Kayabali, K. (2020), "Investigation of the effect of grain size on liquefaction potential of sands", *Geomech. Eng*., **20**(3), 243-254. https://doi.org/10.12989/gae.2020.20.3.243.

Tsaparli, V., Kontoe, S., Taborda, D.M. and Potts, D.M. (2016), "Vertical ground motion and its effects on liquefaction resistance of fully saturated sand deposits", *Proc. Math. Phys. Eng. Sci*., **472**(2192), 20160434. https://doi.org/10.1098/rspa.2016.0434.

Vaid, Y., Stedman, J.D. and Sivathayalan, S. (2001), "Confining stress and static shear effects in cyclic liquefaction", *Can. Geotech. J.*, **38**(3), 580-591. https://doi.org/10.1139/t00-120.

Vaid, Y.P. and Chern, J.C. (1985), "Cyclic and monotonic undrained response of saturated sands", Advances in the Art of Testing Soils Under Cyclic Conditions, Detroit, Michigan, United States,

Vaid, Y.P., Chung, E.K.F. and Kuerbis, R.H. (1989), "Preshearing and undrained response of sand", *Soils Found*., **29**(4), 49-61. https://doi.org/10.3208/sandf1972.29.4_49.

Vaid, Y.P. and Sivathayalan, S. (1996), "Static and cyclic liquefaction potential of Fraser Delta sand in simple shear and triaxial tests", *Can. Geotech. J*., **33**(2), 281-289. https://doi.org/10.1139/t96-007.

Wichtmann, T., Niemunis, A. and Triantafyllidis, T. (2006), "Experimental evidence of a unique flow rule of non-cohesive soils under high-cyclic loading", *Acta Geotech.*, **1**(1), 59-73. https://doi.org/10.1007/s11440-006-0006-8.

Yang, J. (2004), "Reappraisal of vertical motion effects on soil liquefaction", *Géotechnique*, **54**(10), 671-676. https://doi.org/10.1680/geot.2004.54.10.671.

Yang, J., Liang, L.B. and Chen, Y. (2022), "Instability and liquefaction flow slide of granular soils: the role of initial shear stress", *Acta Geotech*., **17**(1), 65-79. https://doi.org/10.1007/s11440-021-01200-1.

Yang, J., Sato, T., Savidis, S. and Li, X.S. (2002), "Horizontal and vertical components of earthquake ground motions at liquefiable sites", *Soil Dyn. Earthq. Eng*., **22**(3), 229-240. https://doi.org/10.1016/s0267-7261(02)00010-6.

Yang, J. and Sze, H.Y. (2011), "Cyclic behaviour and resistance of saturated sand under non-symmetrical loading conditions", *Géotechnique*, **61**(1), 59-73. https://doi.org/10.1680/geot.9.P.019.

Yang, J. and Sze, H.Y. (2011), "Cyclic strength of sand under sustained shear stress", *J. Geotech. Geoenviron. Eng*., **137**(12), 1275-1285. https://doi.org/10.1061/(asce)gt.1943-5606.0000541.

Yang, Z.X. and Pan, K. (2017), "Flow deformation and cyclic resistance of saturated loose sand considering initial static shear effect", *Soil Dyn. Earthq. Eng*., **92**(9), 68-78. https://doi.org/10.1016/j.soildyn.2016.09.002.

GC

List of symbols

C_c	Coefficient of gradation
C_u	Uniformity coefficient
CSL	critical state line
CSR	Cyclic stress ratio
CRR_n	Cyclic resistance ratio
D_r	Relative density
EPWP	Excess pore water pressure
f	Loading frequency
G_s	Specific gravity
K_α	Parameter defined in Eq. (5)
N_f	Number of cycles for failure
p_0'	Initial effective mean stress
q_{cyc}	Amplitude of cyclic deviatoric stress
q_s	Static deviatoric stress
SSR	Shear stress ratio
u_r	Residual excess pore water pressure ratio
ρ_{max}, ρ_{min}	Maximum and minimum dry density
ε_{ar}	Residual axial strain
τ_s	Static shear stress
σ_v, σ_h	Vertical and horizontal stress
σ_v', σ_h'	Effective Vertical and horizontal stress
σ_3^{cyc}	Cyclic spherical stress